Form Segmentation:
An Electrostatic Field-Based Approach

TANYA GRIGORISHIN and YEE-HONG YANG [1]

Computer Vision and Graphics Laboratory

Department of Computer Science

University of Saskatchewan

Saskatoon, Saskatchewan

Canada S7N 5A9

Email Address for Y.H. Yang: yang@cs.usask.ca

Phone Number for Y.H. Yang: (306) 966-4891

Fax Number for Y.H. Yang: (306) 966-4884

June 23, 1997

Abstract

Form segmentation is one of the fundamental tasks for many problems in scene analysis and object recognition. It is a relatively new area of research. The purpose of form segmentation is to distinguish between object parts. It is used to classify objects into classes and hierarchies.

This paper introduces a novel and unique technique for form segmentation of binary, grey level, and colour images. The proposed approach relies on the Electrostatic Field Theory (EFT). It possesses a number of desirable features that naturally solve many problems, some of which have challenged existing form segmentation. In particular, it is capable of performing segmentation under different scales, providing different levels of abstraction. The proposed approach is robust in the presence of severe boundary noise. The experimental results are encouraging.

[1] Author to whom correspondence should be addressed.

1 Introduction

Many of us take for granted our ability to see. We are able to perceive shapes, textures and colours, and are able to process the information in order to understand the surrounding environment. The understanding we gain from looking out at the world is not automatic, however. The human brain processes information in order to attain the awareness and understanding of the environment. If the information is processed incorrectly, we will misinterpret what we see. This misperception may result in various kinds of illusions, e.g. the Herring grid and the Kanizsa triangle [18].

Computer vision attempts to duplicate the success of human vision while avoiding the failures. Eventually it is hoped that machine vision will surpass human perceptual ability. The current level of sophistication of computer vision research faces some challenges and demostrates the complexity of the task of automation of human-like visual capabilities.

Image processing, remote sensing, and industrial automation are the principal areas of computer vision research. These areas employ scene analysis and pattern recognition, where one uses a computer to extract high-level information from an image.

Form segmentation is one of the fundamental tasks for many problems in scene analysis and object recognition. The purpose of form segmentation is to distinguish between object parts [10]. It is used when classifying objects into classes and hierarchies. A variation of the task of form segmentation has been applied in motion tracking [14], [13].

Form segmentation is a relatively new area of research. Most techniques are applicable only to binary images [26]. The developed approaches face problems of noise sensitivity. Some produce intuitive results which depend on the local object properties [10].

The main contibution of this paper is to propose a novel approach that performs the task of form segmentation. The proposed approach is based on the Electrostatic Field Theory (EFT). This paper shows that the EFT presents a natural solution for form segmentation problem. It allows a multi-scale representation and noise sensitivity.

The organisation of this paper is as follows. Section 2 presents an overview of the related research in the area of image form segmentation. Section 3 introduces the EFT background. A novel EFT-based approach for form segmentation is described in Sections 4. The experimental results are discussed in Section 5. Finally, conclusions and future extensions are presented.

2 Related Work

Recent work in the area of form segmentation can be classified into two categories: region-based segmentation and contour-based segmentation.

The *region-based* partitioning methods are based on the decomposition of the interior region rather than on the segmentation of its boundary. Some region-based approaches decompose the region along the maximally convex parts [24], other use a description-based combination of primitives such as cylinders [20], or use a description in some language [22]. Blum [3], [4] propose to partition the object along its skeletal branches.

In contrast to the techniques of the first category, the *contour-based* methods use boundary features such as high-curvature points [7] to perform the task of form segmentation. However, they do not detect object parts which are not derived from curvature extrema of the boundary, that is, neck-based [25] parts of the objects.

The information contained in the image can be represented as regions or by the boundaries of regions. According to Cavanagh [6], humans have more difficulty recognising images with line drawings than with region information. Contour-based methods require the original image to be represented as the boundaries of the regions. To do this, the boundary information has to be extracted prior to form segmentation. Boundary detection is a difficult process, in particular, when the regions are not well defined because of the presence of discontinuities or noise. Therefore, the region-based methods are considered to be more promising than the techniques that require edge detection.

Another way to classify form segmentation techniques is to divide them into methods that are primitive-based and non-primitive based.

Primitive-based partitioning methods approximate the boundary or the interior of the region using such primitives as polygons, primitive curvature changes, e.g. bends, cranks, ends, etc. [2]. The techniques in this category usually have limited capabilities, whether they are applied to the boundary of the region or to the region itself.

Different form segmentation techniques use different representations of the segmented shape. Hoffman and Richards' boundary-based technique [10] leads to a representation of the shape boundary as *codons*. Codons are the segments of the boundary separated by negative curvature minima. This method uses the curvature maxima and zeros to classify each segment as one of the six possible types [23]. In contrast to the primitive-based methods, Hoffman and Richard's technique suggests that the decomposition of the object should precede the description of the object.

Leyton [15] represents the resulting shape not as a collection of rigid segments, but as an explanation based on a consequence of historical processes (Symmetry-Curvature Duality Principle) [16].

Kimia, Tannenbaum, and Zucker [12] propose a combination of shape representations. The clearly defined parts of the object are represented as segments. Other parts, such as the extreme protrusions, are described as other objects. An advantage of this method is that it detects neck-based parts of the object. For a more detailed description consult [12].

A difficult problem with current form segmentation approaches is the ability to detect the bottom-up/top-down bottleneck parts [26]. Many approaches do not study the behaviour of the segmentation process under different scales. According to Siddiqi and Kimia [26], a partitioning scheme should be stable with respect to changes in resolution. When moving from a fine to a coarse scale, parts are only removed, not added. Little research has been done to study the sensitivity of form segmentation techniques to noise and the performance of segmentation in the cases of uneven illumination in an image. The developed approaches work for binary images only.

3 Background on the EFT

This section reviews the general concepts of the EFT. For a more detailed description consult [27], [21].

1. Let us consider two charged particles separated by a fixed distance R. According to Coulomb's Law, the force acting along the line between two charges can be expressed in the following vector equation:
$$\vec{F} = C \ \frac{Q_1 Q_2}{R^2} \ \vec{r},$$
where Q_1 and Q_2 are the magnitude of charges, R is the distance between charges, and C is a constant which depends on the medium, $\vec{r}$ is a unit vector

2. The entire region of influence of a charge is called the electrostatic field. Its magnitude is specified by a quantity called the electrostatic field intensity and is denoted by symbol E. The field intensity is defined as the force per unit charge exerted on a given charge in the field, or
$$\vec{E} = \frac{\vec{F}}{Q} = C \ \frac{Q}{R^2} \vec{r}.$$
The corresponding potential distribution may be found as
$$v = C \ \frac{Q}{R}.$$

3. The electrostatic field intensity vector $\vec{E}(x, y)$ can be computed from the potential $v(x, y)$ as:
$$\vec{E} = -\nabla v.$$
The following observations can be made: the field is in the direction of the steepest descent of the potential; the field lines are perpendicular contours and are directed from the high to the low potential.

4. The electrostatic field conveys the same information as the curvature of an object boundary, which has been verified both theoretically and experimentally [19]. Electrostatic field extrema along an equipotential contour correspond to curvature extrema: significant convexities and concavities [1].

4 Form Segmentation using EFT

This section presents a novel EFT-based algorithm for form segmentation.

In the proposed EFT-based segmentation scheme for binary or grey level images all points of the objects are modelled as unit charges. For a binary case, the values of the charges are set to 255 (see Figure 1(a)). For a grey level image, the values of the charges are defined by the intensity values of the image points (see Figure 1(b)).

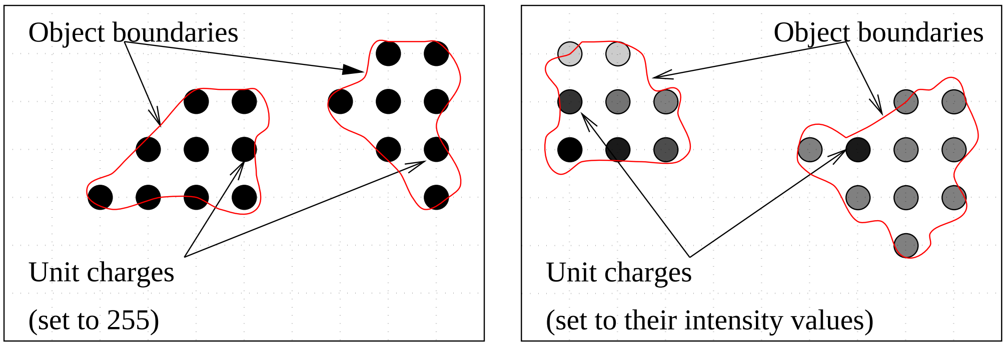

(a) (b)

Figure 1: The EFT-based image model: (a) for a binary image; (b) for a grey level image.

For colour images, each of the red, green, and blue colour channels are processed independently using the same technique as proposed for binary or grey level images. The final segmentation results are then obtained as a union of the segmented regions for each of the three colour channels.

The following steps are required to perform the task of form segmentation for binary or grey level forms:

1. Compute the potential map $V_{main} = V(x, y)$ of the original form. The computation of the potential map is adopted according to the method described in Section 4.1.

2. Detect the equipotential contours at a specified potential level v_{con1}. Retrieve the regions that are outlined by the detected equipotential contours. Uniformly expand the retrieved regions in all directions until the boundary of the original object is reached. This processes is referred to as a *region growing process*. The region obtained by a region growing process is called a *main region* of an object, since it defines the central part of an object.

   The purpose of the following steps is to segment the remaining regions of an object, by adopting a similar technique as that described in steps 1 and 2. In this paper these remaining regions are called *secondary regions* of an object.

3. Compute the second potential map $V_{sec} = V(x, y)$ of the object given by the intersection of the original object and a main region.

4. Find all the equipotential contours at a specified potential level v_{con2}. Retrieve the regions that are outlined by these equipotential contours and adopt a region growing process. The purpose of a region growing process is to expand the retrieved regions to fit the boundaries of the original object. The regions obtained after a region growing process are the secondary regions of an object.

The following sections describe the details of each of the above steps.

4.1 Solution of the Potential Distribution

The presented method of computation of the potential distribution $V = v(x, y)$ uses a predefined structuring element. The structuring element K is of the same size as the image. The origin is at the centre of the structuring element. The value of the element at location (x, y) is

$$\frac{1}{(x^2+y^2+depth^2)^\alpha},$$

where *depth* is an integer number that defines the viewing distance from the image plane ($depth \geq 1$), α is a real number parameter defined by the user ($\alpha \geq 0.5$). The influence of these parameters on the behaviour of the potential map is studied in Section 4.4.

The value of the element at location (x, y) gives the contribution of a unit charge located at (x, y) because the electrostatic potential $v(x, y)$ at the centre is inversely proportional to the distance between (x, y) and the centre of the mask. Hence, the total potential at the centre of the mask is the summation of all the potentials due to charges within the neighbourhood of the mask.

The potential distribution is given by the convolution of K with the input image, which can be computed efficiently using the Fast Fourier Transform (FFT). The FFT of K is computed and then it is pointwise multiplied with the FFT of the input image. The inverse FFT is then performed to obtain the potential field distribution of the image.

After the potential distribution is computed, it is normalised as follows. The potentials outside the objects boundaries are set equal to 0. The maximum potential is set equal to 255. The potential values inside the objects are computed using a simple linear transformation.

In this section the binary image of a hand is used to illustrate the details of the EFT-based approach for form segmentation. Figure 2 depicts the original binary image of a hand, the potential map generated for this image.

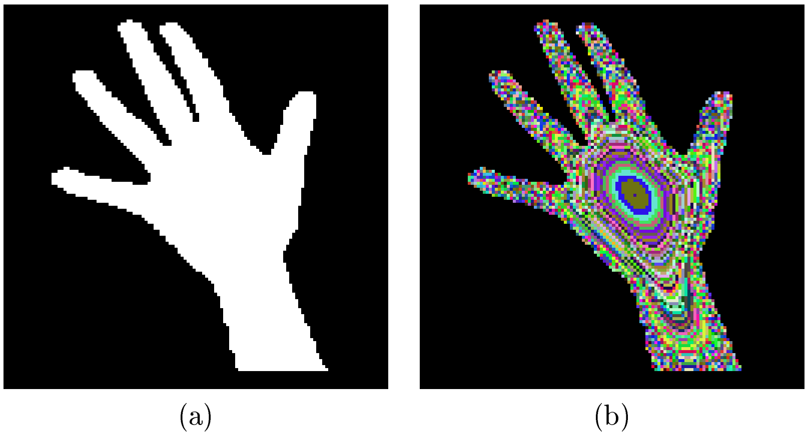

Figure 2: Computation of the potential map V_{main} for the image of a hand. (a) Original image. (b) Generated potential map V_{main}. Parameters: $\alpha = 1$, $depth = 1$.

4.2 Detection of the Equipotential Contours at a Given Potential

The equipotential contours at a given potential, v_{con} within the range 0 - 255, are constructed from the computed potential map. This step can be visualised as a 3D surface $V = v(x, y)$ being cut by a constant potential plane (parallel to the x-y plane). The curves that result from the intersection of the potential surface and the cutting plane are closed equipotential contours at a given potential. These equipotential contours outline the regions in the image.

It is worth nothing that the higher the value of the contour potential v_{con}, the closer the contours are located to the boundaries of the objects. Figure 3 depicts the some equipotential contours constructed for the image of a hand at various potentials. For the higher potential value of 240, the equipotential contours outline the central parts of the image regions. The equipotential contours at a lower potential value of 30 are located closer to the regions' boundaries. This is an interesting property, particularly for the images with a severe boundary noise for the image objects.

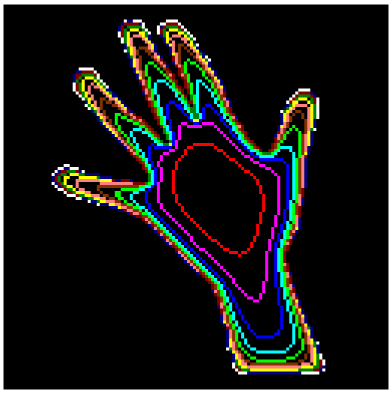

Figure 3: Equipotential contours constructed in the range 0 - 255 in steps of 20 for the potential map depicted in Figure 2(b).

The regions that correspond to the equipotential contours at a given potential are defined as follows:

$$R = \{R_1(s), R_2(s), \ldots, R_k(s), \ldots, R_n(s)\},$$

where n is the number of regions, $R_k(s) = \{(x, y) \mid v_{con} \leq v(x, y)\}$, $k = 1, 2, \ldots, n$, and $v(x, y)$ is the potential at location (x, y).

Figure 4(a) illustrates the retrived regions that are outlined by the detected equipotential contours at the potential $v_{con1} = 230$. The results of the region growing process are shown in Figure 4(b).

(a) (b)

Figure 4: Detection of the main region of the image of a hand. (a) Region outlined by the equipotential contour at the potential $v_{con1} = 230$; (b) The result of a region growing process, i.e. main region.

4.3 Detection of the Secondary Regions

The purpose of this step is to segment the secondary regions of an object. First, the potential map V_{sec} is computed for the intersection of the original image and a main region (see Figure 5). Next step is to detect the regions at a specified potential v_{con2} and adopt a region growing process expand these regions. Figure 6 depicts the details of this step as well as the final results of the EFT-based form segmentation.

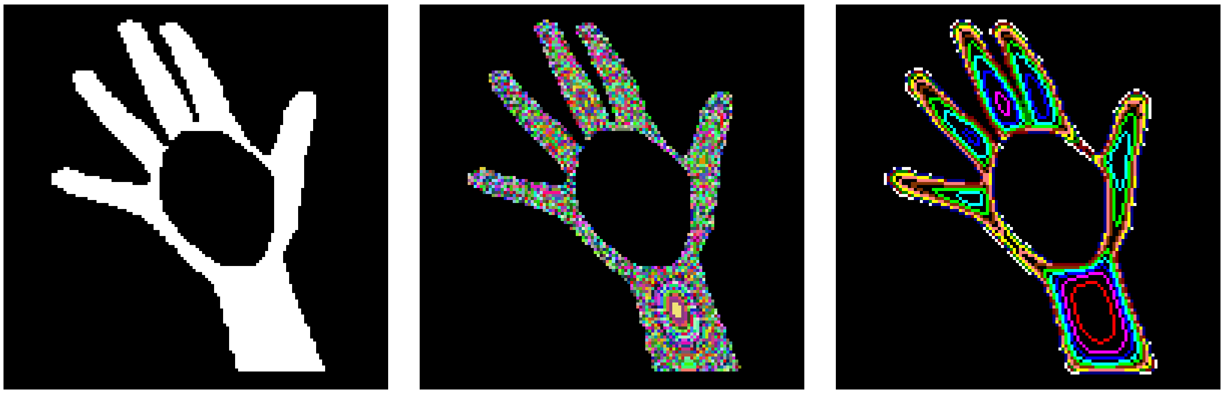

(a) (b) (c)

Figure 5: Computation of the potential map V_{sec} for the image of a hand. (a) Intersection of the original object and the main region. (b) Generated potential map V_{sec}. Parameters: $\alpha = 1$, $depth = 1$. (c) Equipotential contours constructed in the range 0 - 255 in steps of 20.

(a) (b) (c)

Figure 6: Detection of the secondary regions and form segmentation results for the image of a hand. (a) Regions outlined by the equipotential contours at the potential $v_{con2} = 130$. (b) Results of a region growing process adopted for these regions, i.e secondary regions. (c) Form segmentation results.

4.4 Effect of User Defined Parameters on the Behaviour of a Potential Map

A larger value of α reduces the influence of the charges that are located at a greater distance and increases the contribution of the neighbouring charges. Therefore, a larger value of α forces the equipotential contours to be located closer to the regions' boundaries. Figure 7 illustrates the influence of parameter α on the behaviour of the equipotential contours.

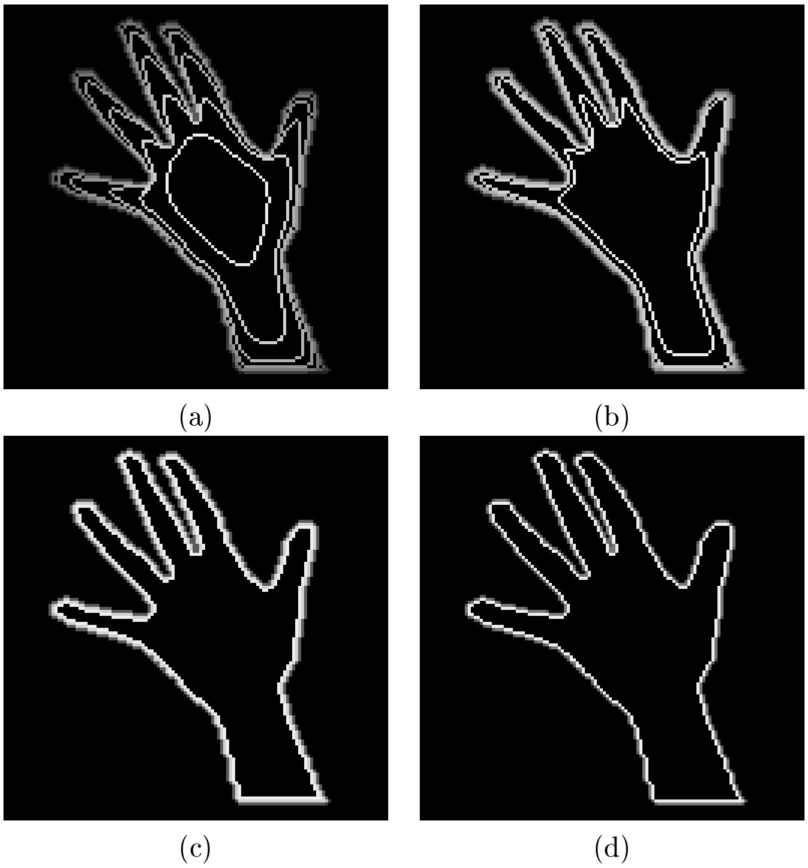

Figure 7: Effect of the α parameter. The equipotential contours shown are constructed in the potential range 0 - 255 in steps of 30, parameter *depth* = 1. (a) $\alpha = 1$; (b) $\alpha = 1.5$; (c) $\alpha = 3$; (d) $\alpha = 5$.

By appropriately choosing the value of a viewing distance from the image plane, *depth*, the desired level of detail (or scale) of the segmentation can be selected. In particular, choosing a larger value of *depth*, a coarse segmentation is generated, whereas a smaller value of *depth* results in a fine segmentation process. The effect of the *depth* parameter on the behaviour of the equipotential contours is illustrated in Figure 8.

It is worth noting that the behaviour of the EFT-based form segmentation process

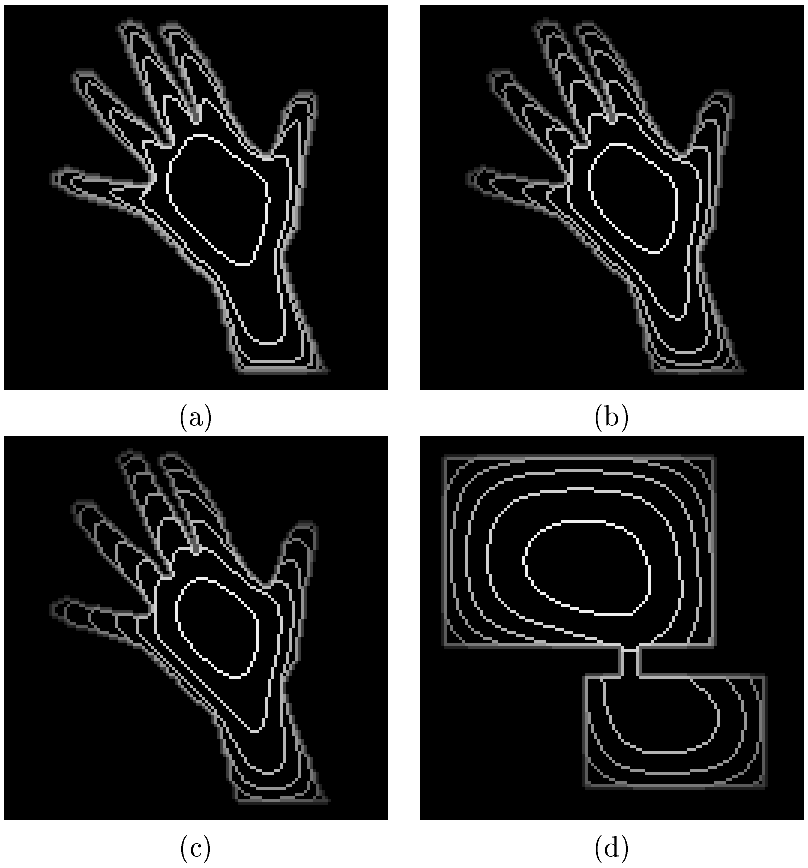

Figure 8: Effect of the *depth* parameter. The equipotential contours shown are constructed in the potential range 0 - 255 in steps of 30, parameter $\alpha = 1$. (a) $depth = 1$; (b) $depth = 3$; (c) $depth = 5$; (d) $depth = 10$.

is dependent upon the selection of the potentials v_{con1} and v_{con2}. The larger value of v_{con1} results in the equipotential contours being closer to the central part of an object. The smaller value of v_{con1}, the larger are the regions that correspond to the detected equipotential contours (see Figure 9). Figure 10 illustrates the main regions generated by the region growing process from the corresponding images displayed in Figure 9. One can clearly see that it is important to choose the appropriate value of v_{con1}. The selection of the potential v_{con1} can be application dependent or it can be set to the value of the highest potential on the boundary of an object.

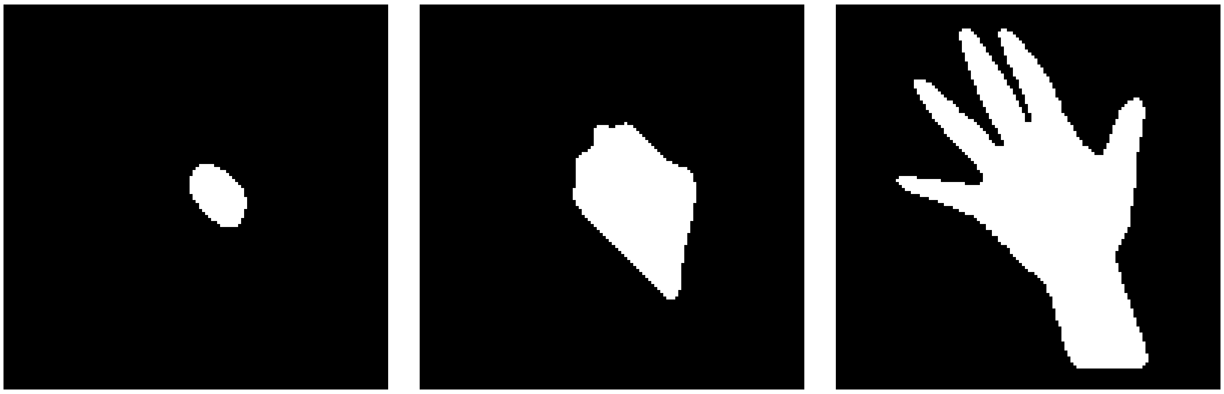

(a) (b) (c)

Figure 9: Effect of the potential v_{con1}. Regions outlined by the equipotential contours detected at different potential v_{con1} for the image of a hand: (a) $v_{con1} = 250$; (b) $v_{con1} = 220$; (c) $v_{con1} = 100$.

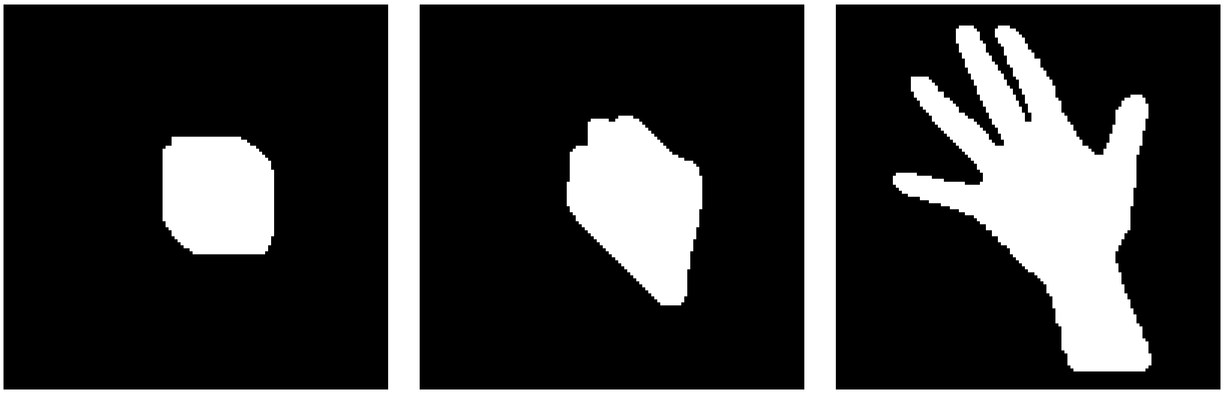

(a) (b) (c)

Figure 10: Main regions of the image of a hand detected at different potential v_{con1}: (a) $v_{con1} = 250$; (b) $v_{con1} = 220$; (c) $v_{con1} = 100$.

The potential v_{con2} defines the segmentation scale of the secondary regions. Figure 11 illustrates the regions outlined by the detected equipotential contours at different potential v_{con2}. The corresponding results of the region growing process are depicted in Figure 12. Figure 13 illustrates the final results of the form segmentation process. Figure 14 shows the number of the regions detected for the image of a hand using different potential v_{con2}.

The values of v_{con1} and v_{con2} can be selected so that the maximum number of regions or a certain number of regions is detected. These parameters provide flexibility and multi-scale representation of the segmentation process. The multi-scale representation enables us to represent the segmented image at different levels of abstraction; hence, the algorithm is more noise resistant.

(a) (b) (c)

Figure 11: Effect of the potential v_{con2}. Regions outlined by the equipotential contours detected at different potential v_{con2} for the hand object intersected with a main region. The main region was detected at a potential $v_{con1} = 240$. (a) $v_{con2} = 230$; (b) $v_{con2} = 180$; (c) $v_{con2} = 140$.

(a) (b) (c)

Figure 12: Secondary regions of the image of a hand detected at different potential v_{con2}. The main region was detected at the potential $v_{con1} = 240$. (a) $v_{con2} = 230$; (b) $v_{con2} = 180$; (c) $v_{con2} = 140$.

Let us consider the behaviour of the proposed method for composite objects, i.e. objects with neck-based parts. Figure 15 illustrates an example of a composite object, the main regions detected and the remaining regions.

Figure 16 illustrates the form segmentation results for the image of a composite object using different potential v_{con2}. the effect of the potential v_{con2} on the number of segmented regions for the image of a composite object is shown in Figure 17. From the above examples, two observations can be made:

1. For some values of the potential v_{con2}, the incorrect regions are detected. It is expected since the second potential map (see Figure 18) is computed for the image

(a) (b) (c)

Figure 13: Form segmentation results of the image of a hand using different potential v_{con2}. The main region was detected at the potential $v_{con1} = 240$. (a) $v_{con2} = 230$; (b) $v_{con2} = 180$; (c) $v_{con2} = 140$.

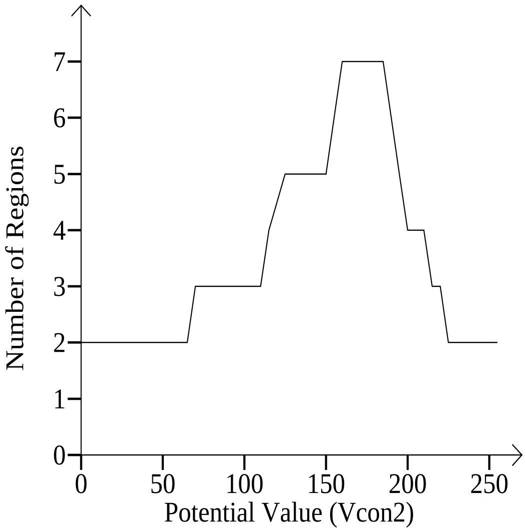

Figure 14: Effect of the potential v_{con2} on the number of segmented regions for the image of a hand. The value of v_{con1} is set to 240.

given by the intersection of the original object and a main region. The intersected image contains secondary regions as well as the undetected parts belonging to the main region. This effect can be avoided by selecting a larger value of α when generating a potential map (see Section 5.2 for more details).

2. The proposed EFT-based approach for form segmentation does not detect neck-based parts of an object as a separate region. This is expected because of the nature of the potential map.

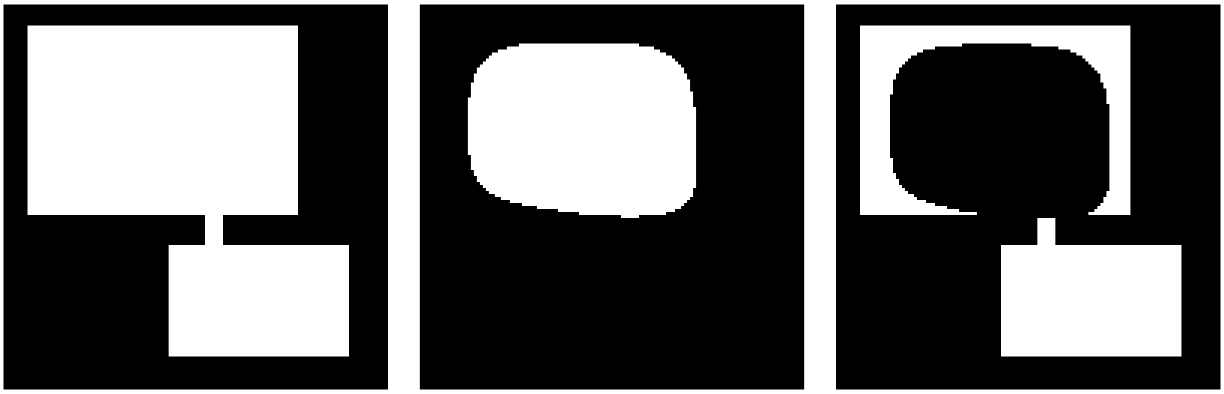

(a) (b) (c)

Figure 15: Form segmentation of the image of a composite object. (a) The original image of a composite object. (b) One main region detected at the potential $v_{con1} = 220$. (c) Remaining regions.

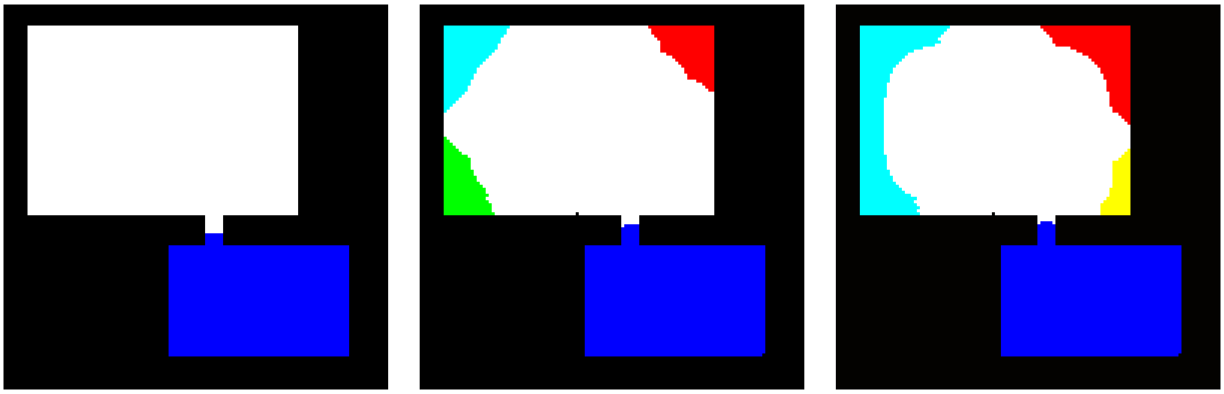

(a) (b) (c)

Figure 16: Form segmentation of the image of a composite object using different potential v_{con2}. The main region was detected at $v_{con1} = 220$. (a) $v_{con2} = 220$; (b) $v_{con2} = 150$; (c) v_{con2}= 125.

From the above discussion, it is evident that the proposed form segmentation method has the advantage of a multi-scale approach. The selection of the appropriate equipotential contours at v_{con1} and v_{con2} will provide the desired level of detail (scale) of the segmentation.

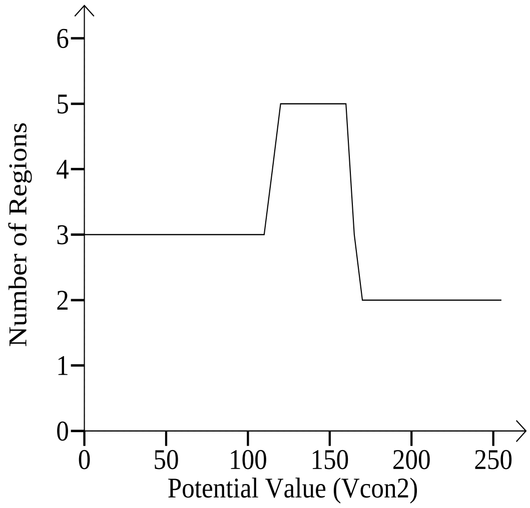

Figure 17: Effect of the potential v_{con2} on the number of segmented regions for the image of a composite object. The value of v_{con1} is set to 220.

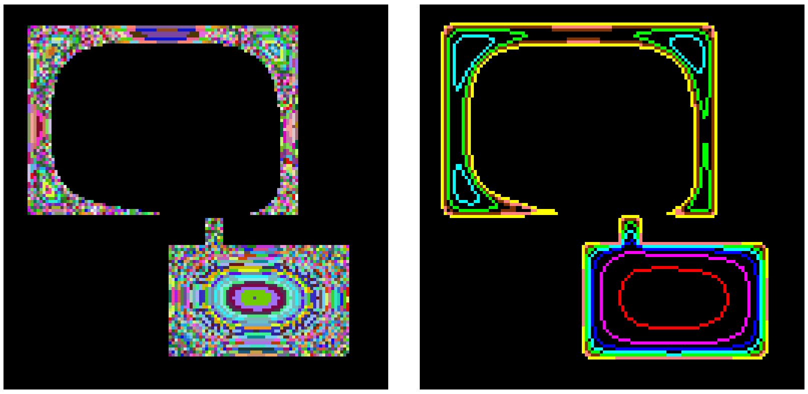

(a) (b)

Figure 18: Computation of the potential map V_{sec} for the image of a composite object. (a) Generated potential map V_{sec}. Parameters: $\alpha = 1$, $depth = 1$. (b) Equipotential contours constructed in the range 0 - 255 in steps of 30.

5 Experiments

To conduct an extensive performance evaluation of the proposed EFT-based approach, a collection of approximately 100 synthesised and real life images have been generated. The size of the generated images is 128 $\times$ 128. Section 5.1 describes the input imagery used to test the performance of form segmentation technique.

The proposed EFT-based approach was tested on a DEC alpha server, model 2100 with 256MB of memory, running OSF/1 V3.0. It is implemented in the C programming language. Tools in the Cantata visual programming environment were also employed [5].

5.1 Input Imagery

To test the performance of the EFT-based form segmentation approach the following input imagery is used:

Scanned grey level images of a cartwheel (see Figure 19(a)). Noisy images are generated by corrupting image boundary with 0-mean Gaussian noise of levels ranging from 0 to 20 in steps of 4. Figures 19(b)-(d) illustrate some of the images generated by this method.

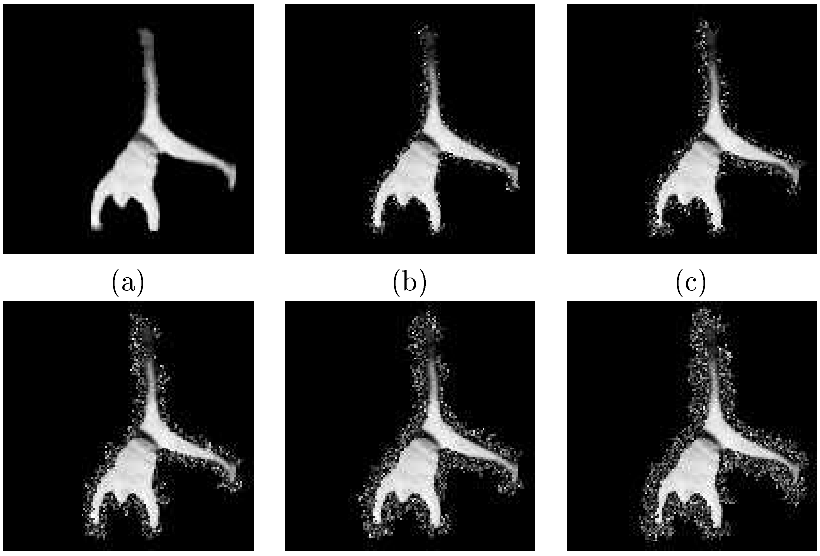

(a) (b) (c) (d) (e) (f)

Figure 19: Original grey level images of a cartwheel with boundary corrupted with a noise of level: (a) $\sigma = 0$ (noise free); (b) $\sigma = 4$; (c) $\sigma = 8$; (d) $\sigma = 12$; (e) $\sigma = 16$; (f) $\sigma = 20$.

5.2 Experimental Results and Performance Analysis

Figure 21 illustrates the results of the EFT-based form segmentation approach for the noise free image of a cartwheel depicted in Figure 19(a). The segmentation results for the noisy images of a cartwheel are illustrated in Figures 22 - 26. Original images corrupted with different levels of boundary noise are shown in Figures 19(b)-(f).

One can clearly see the multi-scale capability of the EFT-based approach. The multi-scale representations can be obtained by changing the values of the potentials v_{con1} and v_{con2}. At a finer scale (smaller values of v_{con1} and v_{con2}), a large number of regions are segmented. At a coarser scale (higher values of v_{con1} and v_{con2}), the segmented object has fewer regions.

The value of the potential v_{con1} defines the number and the shape of the main regions segmented. In segmentation results presented in Figures 22- 26, at the potential $v_{con1} = 240$, only one main region is detected. Two main regions are detected at the potential $v_{con1} = 220$. Note that for the noisy images depicted in Figures 24(e)-(h)- 26(e)-(h) this value of v_{con1} is reduced to 210. This is done because severe boundary noise was added to the images, which requires an increase in the size of the main regions by reducing the value of the potential v_{con1}. The value of v_{con2} defines the number of secondary regions of an object. There is always a trade-off between a suppression of the boundary noise and the number of secondary regions detected. If a low value of the potential v_{con2} is selected, that is, the equipotential contour is located close to the object's boundary, then many small secondary regions are detected. However, some of the regions may not be detected properly because of the presence of noise. For example, the side part of the body trunk in the images in Figures 21(h)- 26(h). On the other hand, if the boundary noise is suppressed, the small regions are not segmented (see Figure 25(h)).

A good form segmentation technique should segment small regions, while suppressing noise as much as possible. It is observed that the form segmentation process is quite insensitive to boundary noise. The noise resistance of the proposed approach can be explained by the nature of the potential map. If the image boundary is corrupted by severe noise, then a larger value of potential v_{con2} should be selected when detecting the secondary regions.

It is also worth noting that in the presence of noise, the small object regions are segmented well by the proposed method. The segmentation of the head is performed correctly, even when the object's boundary is corrupted by severe noise (see Figures 24(d),(h)). The segmentation of small regions of an object is a difficult task, and previously could be achieved only by additional post-processing [13].

The EFT-based approach properly performs the detection of a main region of an object, e.g. the body trunk , which is also a difficult task in the existing form segmentation techniques.

Figure 20 depicts the changes in the selection of the potential v_{con2}, while keeping the number of segmented regions constant. The graph illustrates that in the presence of high boundary noise, the potential v_{con2} should be set higher to preserve the scale of the segmentation process.

The results achived by the proposed approach are very encouraging. This is an original work in the form segmentation area which shows the resistancy of the approach to severe boundary noise and a good performance in the detection of small regions.

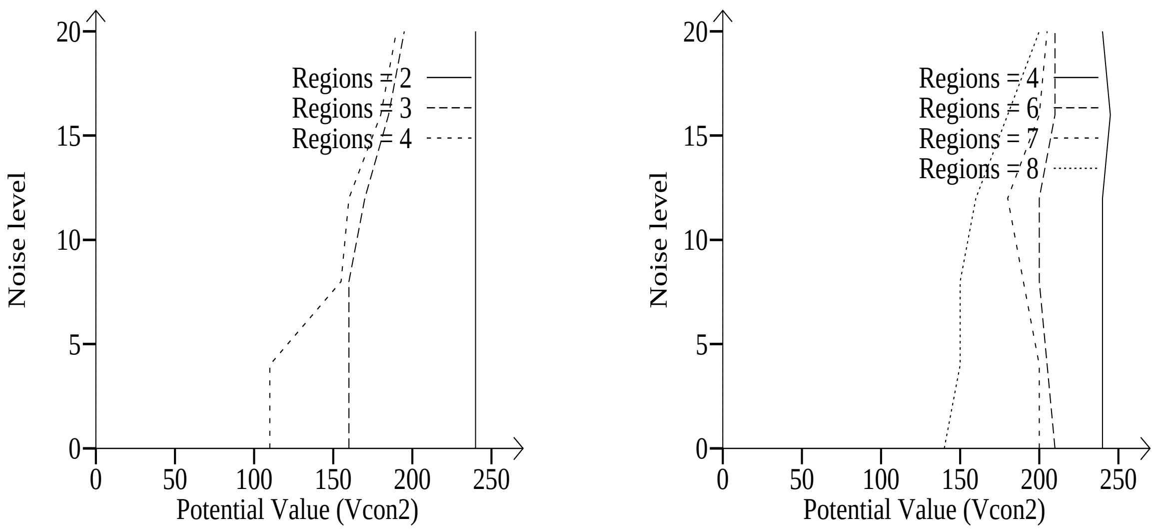

Figure 20: Changes in the selection of the potential v_{con2} versus the noise level. (a) v_{con1} = 240 (one main region detected); (b) v_{con1} = 220 (two main regions detected).

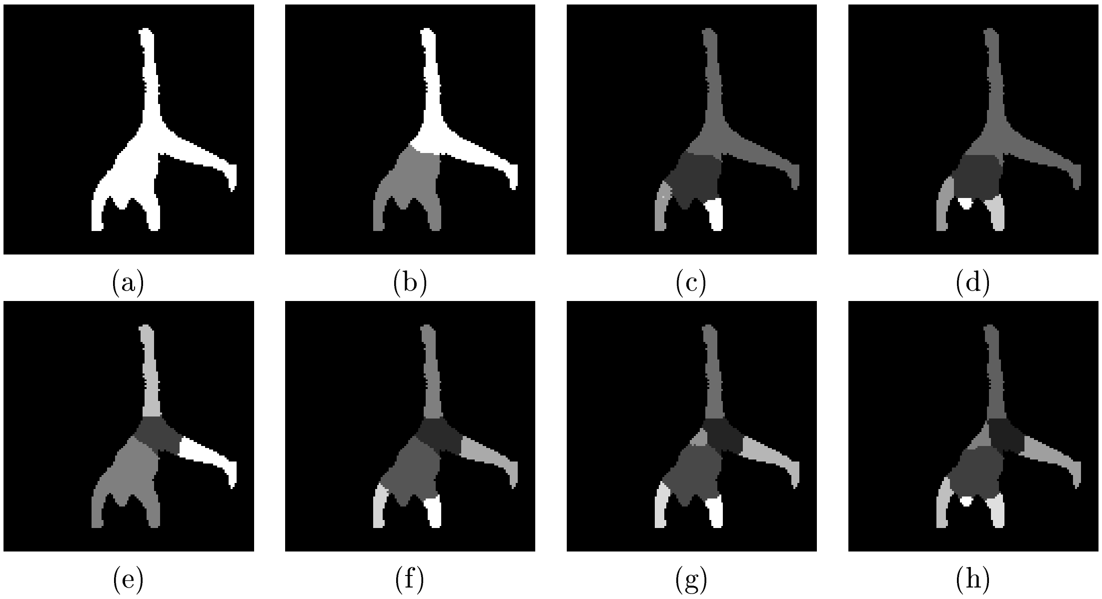

Figure 21: EFT-based form segmentation results for the noise-free image of a cartwheel depicted in Figure 19(a). Parameters: $\alpha = 1$, $depth = 1$. (a) $v_{con1} = 0$, no secondary regions detected; (b) $v_{con1} = 240$, $v_{con2} = 240$; (c) $v_{con1} = 240$, $v_{con2} = 160$; (d) $v_{con1} = 220$, $v_{con2} = 110$; (e) $v_{con1} = 220$, $v_{con2} = 240$; (f) $v_{con1} = 220$,$v_{con2} = 210$; (g) $v_{con1} = 220$, $v_{con2} = 200$; (h) $v_{con1} = 220$, $v_{con2} = 140$.

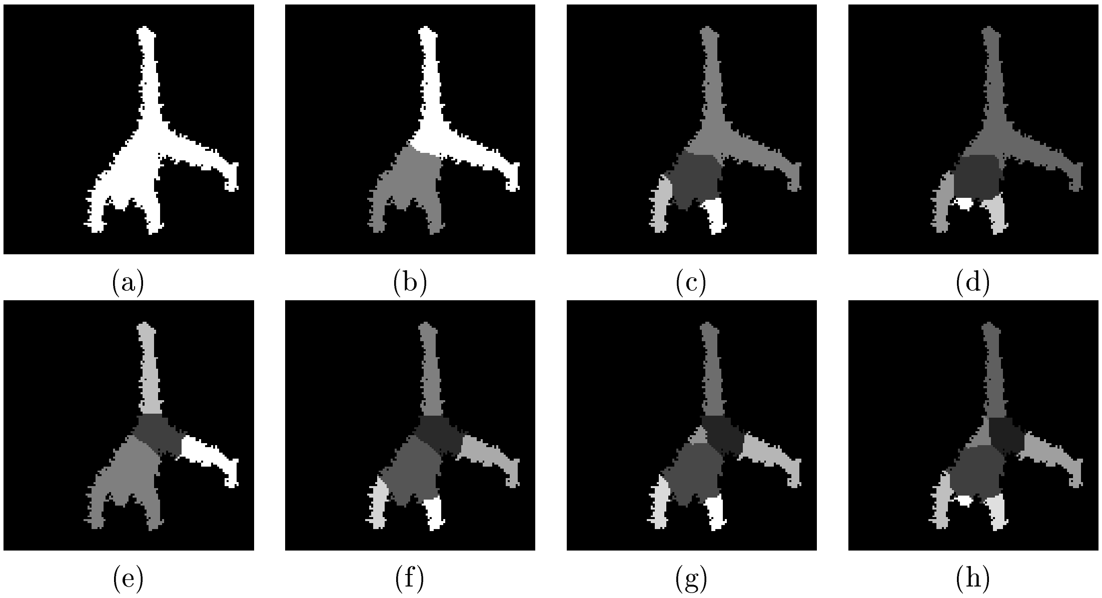

Figure 22: EFT-based form segmentation results for the noisy (σ=4) image of a cartwheel depicted in Figure 19(b). Parameters: $\alpha = 1$, $depth = 1$. (a) $v_{con1} = 0$, no secondary regions detected; (b) $v_{con1} = 240$, $v_{con2} = 240$; (c) $v_{con1} = 240$, $v_{con2} = 160$; (d) $v_{con1} = 240$, $v_{con2} = 110$; (e) $v_{con1} = 220$, $v_{con2} = 240$; (f) $v_{con1} = 220$, $v_{con2} = 205$; (g) $v_{con1} = 220$, $v_{con2} = 200$; (h) $v_{con1} = 220$, $v_{con2} = 150$.

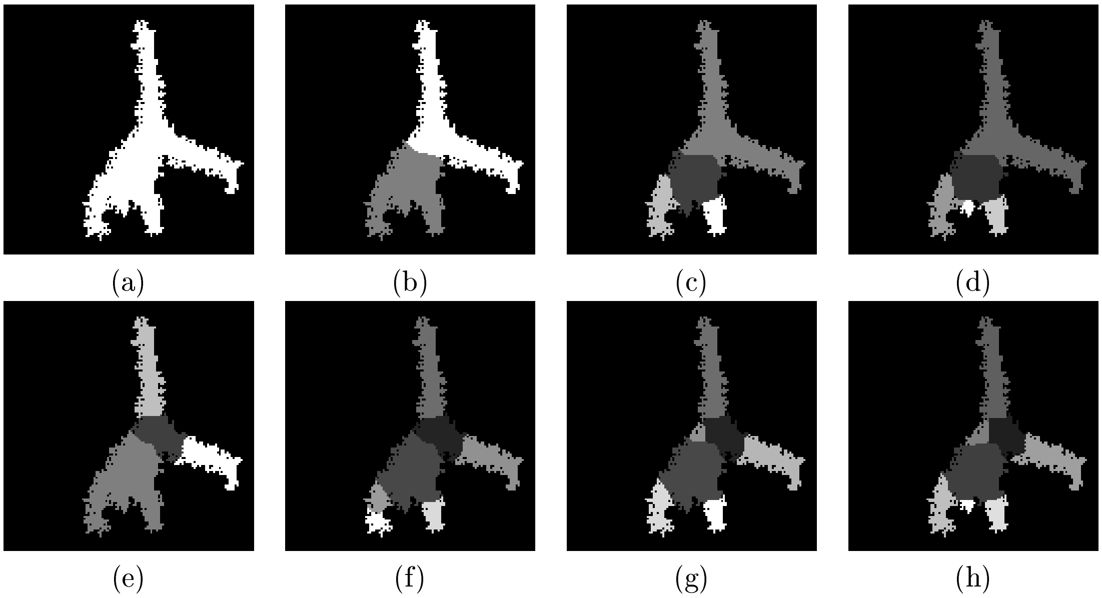

Figure 23: EFT-based form segmentation results for the noisy (σ=8) image of a cartwheel depicted in Figure 19(c). Parameters: $\alpha = 1$, $depth = 1$. (a) $v_{con1} = 0$, no secondary regions detected; (b) $v_{con1} = 240$, $v_{con2} = 240$; (c) $v_{con1} = 240$, $v_{con2} = 160$; (d) $v_{con1} = 240$, $v_{con2} = 155$; (e) $v_{con1} = 220$, $v_{con2} = 240$; (f) $v_{con1} = 220$, $v_{con2} = 200$; (g) $v_{con1} = 220$, $v_{con2} = 190$; (h) $v_{con1} = 220$, $v_{con2} = 150$.

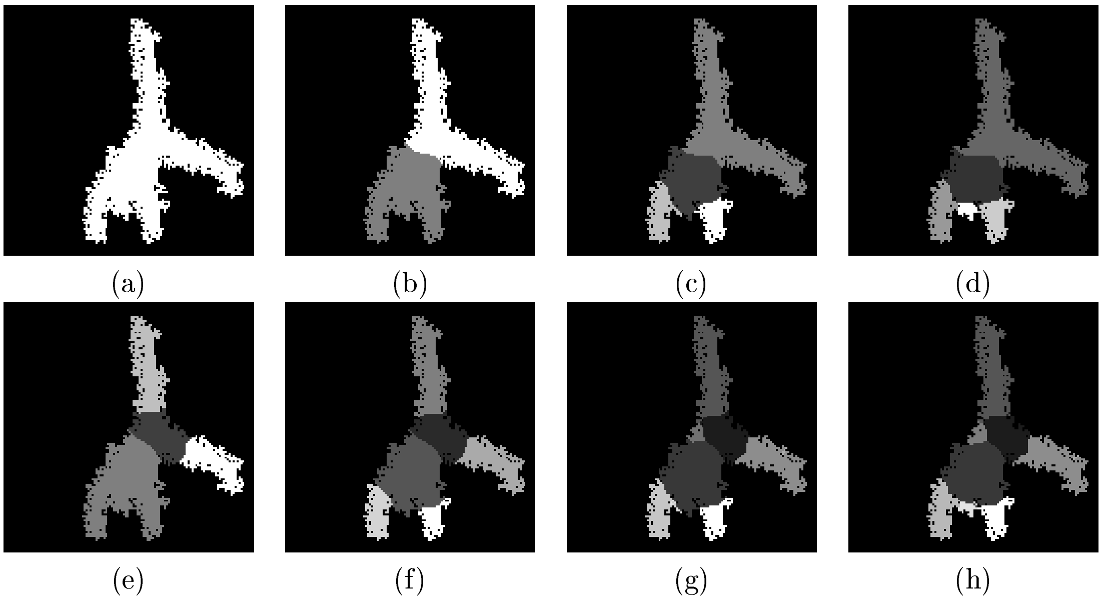

Figure 24: EFT-based form segmentation results for the noisy (σ=12) image of a cartwheel depicted in Figure 19(d). Parameters: $\alpha = 1$, $depth = 1$. (a) $v_{con1} = 0$, no secondary regions detected; (b) $v_{con1} = 240$, $v_{con2} = 240$; (c) $v_{con1} = 240$, $v_{con2} = 170$; (d) $v_{con1} = 240$, $v_{con2} = 160$; (e) $v_{con1} = 210$, $v_{con2} = 240$; (f) $v_{con1} = 210$, $v_{con2} = 200$; (g) $v_{con1} = 210$, $v_{con2} = 180$; (h) $v_{con1} = 210$, $v_{con2} = 160$.

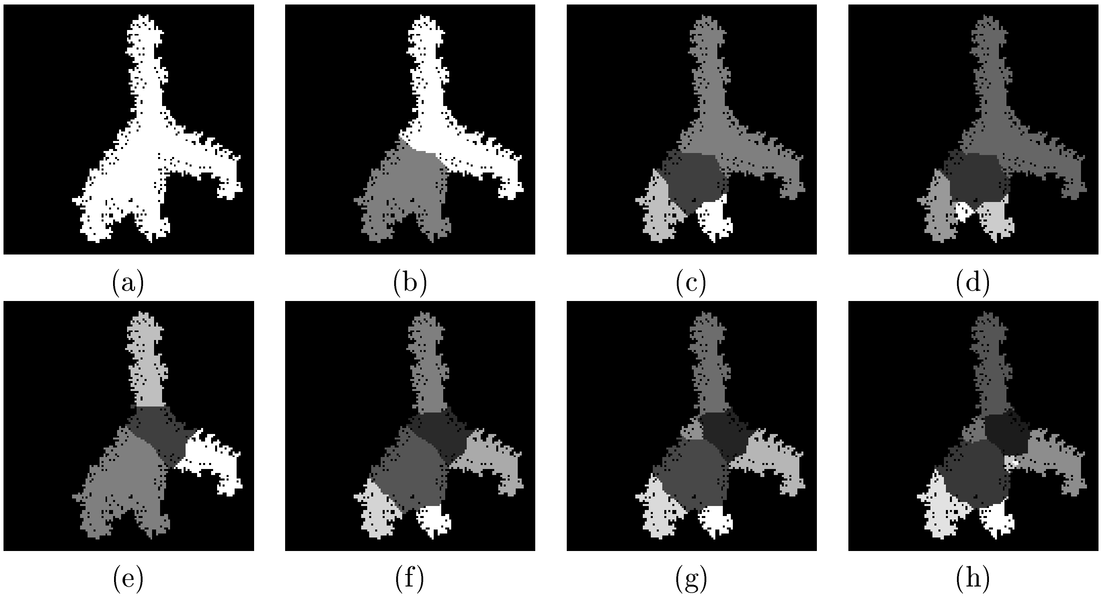

Figure 25: EFT-based form segmentation results for the noisy (σ=16) image of a cartwheel depicted in Figure 19(e). Parameters: $\alpha = 1$, $depth = 1$. (a) $v_{con1} = 0$, no secondary regions detected; (b) $v_{con1} = 240$, $v_{con2} = 240$; (c) $v_{con1} = 240$, $v_{con2} = 170$; (d) $v_{con1} = 240$, $v_{con2} = 160$; (e) $v_{con1} = 210$, $v_{con2} = 245$; (f) $v_{con1} = 210$, $v_{con2} = 210$; (g) $v_{con1} = 210$, $v_{con2} = 200$; (h) $v_{con1} = 210$, $v_{con2} = 180$.

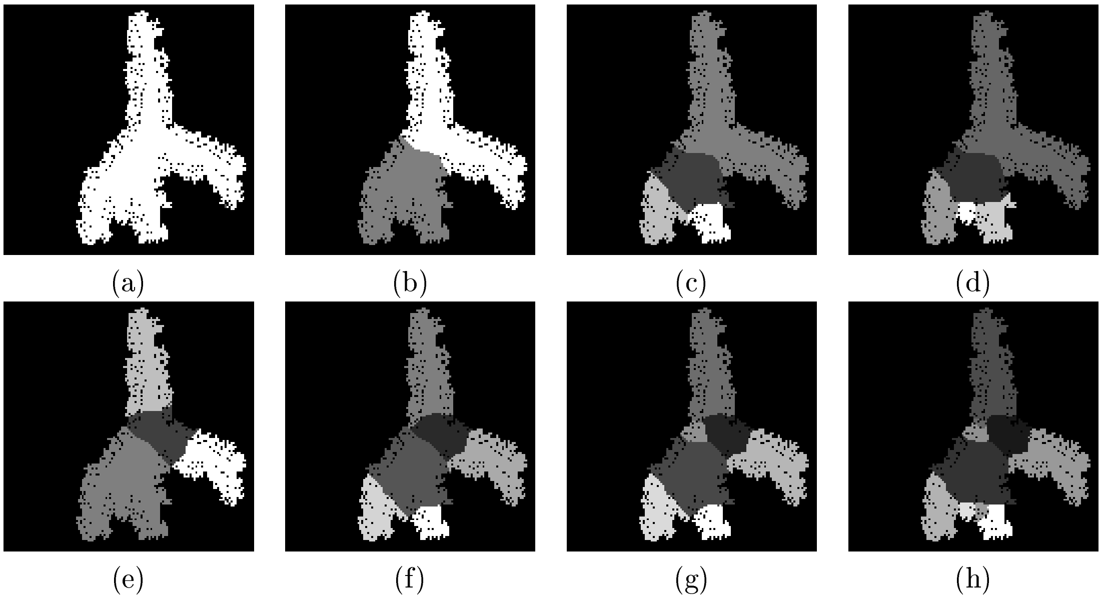

Figure 26: EFT-based form segmentation results for the noisy (σ=20) image of a cartwheel depicted in Figure 19(e). Parameters: $\alpha = 1$, $depth = 1$. (a) $v_{con1} = 0$, no secondary regions detected; (b) $v_{con1} = 240$, $v_{con2} = 240$; (c) $v_{con1} = 240$, $v_{con2} = 195$; (d) $v_{con1} = 240$, $v_{con2} = 190$; (e) $v_{con1} = 210$, $v_{con2} = 240$; (f) $v_{con1} = 210$, $v_{con2} = 210$; (g) $v_{con1} = 210$, $v_{con2} = 205$; (h) $v_{con1} = 210$, $v_{con2} = 200$.

6 Conclusions and Future Work

The problem of form segmentation has been studied in this research. A novel technique for this task of image processing has been introduced. The developed approach possesses a number of desirable features that naturally solve many problems, some of which have challenged existing form segmentation.

The proposed EFT-based approach is capable of performing segmentation under different scales, providing different levels of abstraction. It is robust in the presence of severe boundary noise.

Future work can expand the system to support various colour spaces, such as XYZ, HSV, and others.

Currently, when processing colour images a potential map is computed separately for each of three colour channels and then the results are combined. Future research can examine the computation of a potential map using the ideas borrowed from the opponent theory of colour [8], [9]. The theory suggests that human vision operates on the basis of colour differences. Therefore, it is suggested to examine a potential map for the following colour differences: red and green, green and yellow, i.e. on the basis of the opponent colours.

The proposed algorithm for the detection of a main region of an object can be improved, particularly for the cases when there are two or more subregions in a main region. The detection of the secondary regions of an object is dependent in this model upon the extraneous regions left after the detection of a main region. It is suggested to examine the ways to minimise the error resulting in the improper detection of the secondary regions.

The research work shows that the potential distribution in it own provides a powerful tool for image processing, and inspires further research using the same approach in addressing other vision problems.

References

[1] G. H. Abdel-Hamid and Y. H. Yang. Electrostatic field-based detection of corners of planar curves. In *Proceedings of the 1993 Canadian Conference on Electrical and Computer Engineering*, Vancouver, Canada, pages 767–770, 1993.

[2] H. Asada and M. Brady. The curvature primal sketch. *IEEE Transactions on Pattern Analysis and Machine Intelligence*, 5:2–14, 1983.

[3] H. Blum. Biological shape and visual science. *Journal Theor. Biol.*, 38:205–287, 1973.

[4] H. Blum. Shape description using weighted symmetric axis features. *Pattern Recognition*, 10:167–180, 1978.

[5] Cantata. *Khoros Research Inc.*, 1994.

[6] P. Cavanagh. Reconstructing the third dimension: Interactions between color, texture, motion, binocular disparity, and shape. *Computer Graphics and Image Processing*, 37:171–195, 1987.

[7] H. Freeman. Shape description via the use of critical points. *Computer Graphics and Image Processing*, 10:159–166, 1978.

[8] R. Gershon. A survey on color in computational vision. Technical report, University of Toronto, Department of Computer Science, 1984.

[9] E. Hering. *Outlines of a theory of the light sense.* Harvard University Press, Cambridge, MA, 1964.

[10] D. D. Hoffman and W. A. Richards. Parts of recognition. *Cognition*, 18:65–96, 1985.

[11] D. B. Judd and G. Wyszecki. *Color in Business, Science and Industry.* John Wiley, N.Y., third edition edition, 1975.

[12] B. B. Kimia, A. R. Tannenbaum, and S. W. Zucker. The shape triangle: Parts, protrusions, and bends. Technical report, McGill University Research Center for Intelligent Machines, 1992.

[13] M. K. Leung. *First Sight: Towards a System in Human Body Recognition and Understanding.* PhD thesis, University of Saskatchewan, SK, 1992.

[14] M. K. Leung and Y. H. Yang. An attribute based approach to human body motion analysis. *Int. Journal of Pattern Recognition and Artificial Intelligence*, 5:439–458, 1991.

[15] M. Leyton. Symmetry-curvature duality. *Computer Vision, Graphics and Image Processing*, 38:327–341, 1987.

[16] M. Leyton. Symmetry, causality, mind. Technical report, MIT Press, Cambridge, MA, 1992.

[17] J. Liu. Multiresolution colour image segmentation. Master's thesis, University of Saskatchewan, SK, 1993.

[18] David Marr. *Vision.* W. H. Freeman and Company, N.Y., 1982.

[19] R. Mittra and S. W. Lee. *Analytical Techniques in The Theory of Guided Waves.* McMillan, N.Y., 1971.

[20] R. Nevatia and T. O. Binford. Description and recognition of curved objects. *Artificial Intelligence*, 8:77–98, 1977.

[21] A. Nussbaum. *Field Theory.* Charles E. Merrill Books, Columbus, Ohio, 1967.

[22] A. P. Pentland. Recognition by parts. In *Proceedings of the 1st Int. Conference on Computer Vision*, London, England, pages 612–620, 1987.

[23] W. A. Richards and D. D. Hoffman. Codon constraints on closed 2d shapes. *Computer Vision, Graphics and Image Processing*, 31(2):156–177, 1985.

[24] L. Shapiro and R. Haralick. Decomposition of two-dimensional shapes by graph-theoretic clustering. *IEEE Transactions on Pattern Analysis and Machine Intelligence*, 1:10–20, 1979.

[25] K. Siddiqi. Parts of visual form: Ecological and psychophysical aspects. Technical report, LEMS, Brown University, 1992.

[26] K. Siddiqi and B. B. Kimia. Parts of visual form: Computational aspects. *IEEE Transactions on Pattern Analysis and Machine Intelligence*, 17(3):239–251, 1995.

[27] P. Silvester. *Modern Electromagnetic Fields.* Prentice-Hall, N.J, 1967.